Geophys. J. R. astr. Soc. (1986) **87**, 455–485

Displacement and stress fields produced by a centre of dilation and by a pressure source in a viscoelastic half-space: application to the study of ground deformation and seismic activity at Campi Flegrei, Italy

M. Bonafede, M. Dragoni and F. Quareni *Dipartimento di Fisica, Settore di Geofisica, Universita' di Bologna, Viale Berti Pichat 8, 40127 Bologna, Italy*

Accepted 1986 April 2. Received 1986 April 2; in original form 1985 May 30

Summary. Analytical expressions for the static displacement field produced by a centre of dilation and by a pressure source in a viscoelastic half-space are derived. The associated stress fields are also computed. The rheology of a standard linear solid (SLS) is adopted for the shear modulus, while the incompressibility is kept elastic. An instantaneous dilation or variation of pressure is considered as responsible for the deformation. In the centre of dilation model, if the two rigidities of the SLS are of the same order of magnitude, the viscoelastic contribution to the deformation is negligible; if the short-term rigidity is at least two orders of magnitude higher than the other one, the results are indistinguishable from those obtained with a Maxwell solid rheology. In this case, it is found that the initial elastic displacement is amplified by 20 per cent. In the pressure source model, if the rigidities of the SLS are of the same order of magnitude, the initial elastic displacement is amplified by a factor of about 2, but unrealistically high pressure values are required. On the other hand, for a Maxwell solid rheology the displacement grows indefinitely in time, following a sudden application of a finite pressure. The uplift rate is evaluated and it is shown that, for obtaining values of the order of 1 m over one characteristic relaxation time, more reasonable values of pressure are allowed. Applications to ground deformation in volcanic areas are discussed, taking as an example the Campi Flegrei zone, near Naples, Italy.

Key words: viscoelasticity, deformations in volcanic areas, seismicity

1 Introduction

The elastic deformation due to an isotropic nucleus of strain has been often considered in the geophysical literature. Nuclei of strain are concentrated sources of a displacement field in an elastic medium and are built up from the simple superposition of single forces acting at a point in the medium (Love 1927). The displacement field due to nuclei of strain in a half-

space is necessary for applications to crustal deformation. Analytical expressions for some nuclei of strain in an elastic half-space, including a centre of dilation, were given by Mindlin & Cheng (1950). A complete solution for the fundamental types of nuclei of strain was given by Maruyama (1964), in the case in which the two Lamé parameters λ and μ are equal: this corresponds to a Poisson modulus $\nu = 0.25$, which is appropriate to most of the Earth's crust. The solution for the displacement produced by a centre of dilation is useful for many purposes. Mogi (1958) applied a centre of dilation in an elastic space to interpret the ground deformation produced in volcanic areas and this model is often called the Mogi's model after him. Further applications of Mogi's model to the interpretation of ground deformation in volcanic areas such as Kilauea (Fiske & Kinoshita 1969; Walsh & Decker 1975), Long Valley Caldera (Savage & Clark 1982; Rundle & Whitcomb 1984; Rundle *et al.* 1985), Palmdale (Rundle 1978a) and Campi Flegrei (Corrado *et al.* 1976; Berrino *et al.* 1986). Finite element models with different shapes for the magma chamber were worked out by Dieterich & Decker (1975). This model has been also employed to describe the deformation connected with dilatancy and fluid diffusion (Singh & Sabina 1975; Rundle 1978a) and with underground nuclear explosions (Ben-Menahem & Gillon 1970).

However, for some purposes the anelastic properties of the Earth's crust are to be considered. This is particularly the case in volcanic areas where the presence of incoherent materials and higher temperatures produce a lower effective viscosity of the Earth's crust. A first step is to consider the deformation produced by a nucleus of strain in a viscoelastic medium.

The problem of nuclei of strain in an elastic layer overlying a viscoelastic half-space has been faced by Rundle (1978b) to model the effect of the asthenosphere. However, the presence of two layers with different rheological properties makes the analytical solution difficult to find and one must finally resort to numerical techniques. For a nucleus of strain in a homogeneous viscoelastic half-space the problem is easily solved in an analytical way from the formulae derived by Maruyama (1964) for nuclei of strain in an elastic half-space, with $\lambda = \mu$. However, most rocks flow to relax deviatoric stresses, as though their rigidity decreased gradually with time, while relaxation of the isotropic stress component is usually negligible. For this reason, only the deviatoric stress is treated as viscoelastic, while the isotropic stress is linked through an elastic constitutive relation to isotropic strain. This can be done by choosing the rheologies of the incompressibility K and the rigidity μ independently (e.g. Christensen 1971). In our paper, a standard linear solid (SLS) rheology is adopted for the shear modulus, while K is left as a constant.

In an elastic medium, the deformations produced by a dilation at one point (centre of dilation) coincide with those due to a pressure change applied on the surface of a spherical cavity (centre of pressure), since a pressure change can be associated with a change of volume through the Lamé constants. However, when viscoelasticity is taken into account, different deformations are produced by these two different sources. We shall work out analytical solutions for the displacement field for each one of the two sources in a viscoelastic half-space. For this purpose, the expressions for the elastic displacement field are first derived as done by Maruyama (1964), but keeping $\lambda \neq \mu$. The solution is then rewritten in terms of μ and K and the viscoelastic solution is finally obtained by applying the correspondence principle (Christensen 1971) only to the shear modulus μ. The associated stress fields are also computed from the analytical expressions of displacements.

The model is then applied to the volcanic area of Campi Flegrei, south of Italy. In this century, ground deformations accompanied by seismic activity occurred in the area of Campi Flegrei. Quantitative measures are available from the beginning of 1970, when a ground uplift was detected and continuously monitored by tide-gauges installed in the

central part of the area. The uplift continued with decreasing rate until the summer of 1972, when it reached its maximum, about 60 cm. Then, the ground level began to decrease, although very slowly, and reached a steady value in 1974. After this episode, a similar process involved the Campi Flegrei area, beginning in 1982 and leading to a maximum uplift of about 160 cm, in 1984 September. In Fig. 1, from Berrino *et al.* (1986), the dots represent the measures of ground level in the central part of the caldera, from 1970 to 1983. At the end of 1984, a slow deflation has been detected, probably analogous to the deflation

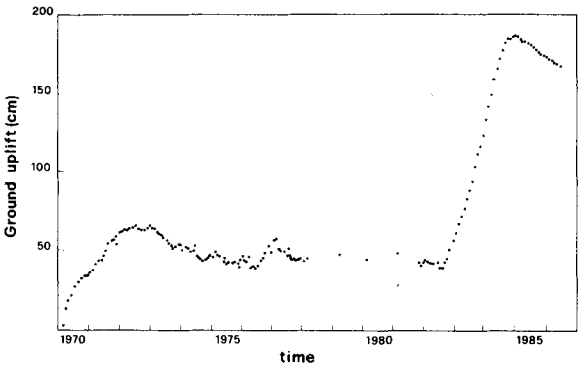

Figure 1. Observed uplift in the central part of the caldera of Campi Flegrei from 1970 till 1986 (redrawn from Berrino *et al.* 1986) and from data courtesy of Osservatorio Vesuviano, Naples.

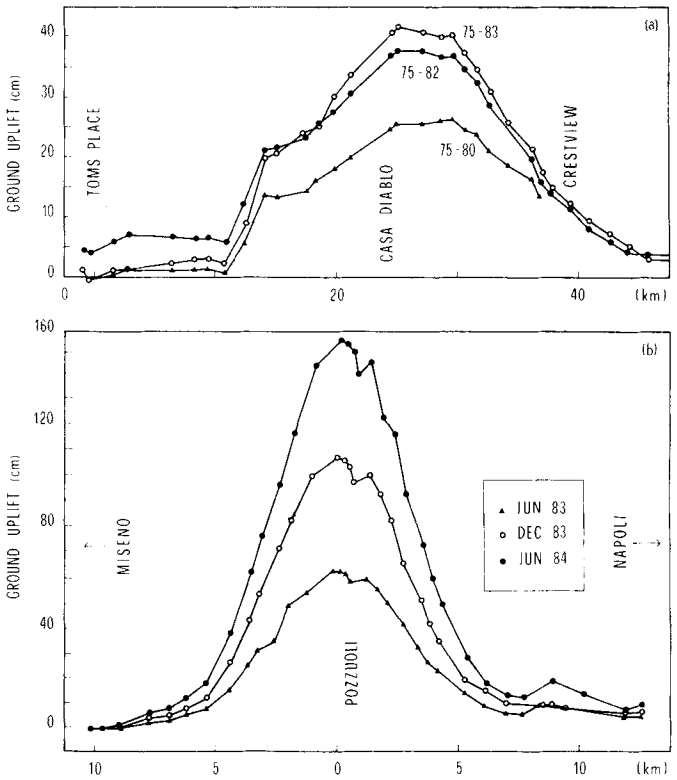

Figure 2. Observed uplift measured at Campi Flegrei, Italy, and Long Valley Caldera, California, as a function of the distance from the point of maximum uplift (redrawn from Berrino *et al.* 1986 and from Rundle *et al.* 1985, respectively).

of 1972–73 (Berrino *et al.*, note presented at the 'Riunione Scientifica sui Campi Flegrei', Naples, 1985 March 28). Seismic activity accompanied both these two deformation processes. The measures of the ground level show a nearly radial symmetry, thus allowing one to use axisymmetric models in order to represent the dynamics of Campi Flegrei. The shape of the gound level curves plotted versus distance from the maximum uplift point is characteristic of volcanic areas: another typical and well-known example is Long Valley Caldera (Fig. 2a). Much evidence suggests that the uplift is related to the existence of a magma chamber at a depth of about 3 km beneath Pozzuoli, having a nearly spherical shape and a radius ranging from some hundreds of metres (Berrino *et al.* 1986) to 1.5 km (Armienti *et al.* 1983). A magma migration involving the upper part of the chamber would provide a pressure increase responsible for the ground uplift.

Furthermore, external tidal and meteorological forces produce additional ground deformations (Palumbo 1985). This shows that the volcanic area is very sensitive even to weak forces, applied for long times, thus suggesting an anelastic behaviour.

Elastic models have been applied to the Campi Flegrei area, both making use of the original analytical solution by Mogi (1958) for a point-like source (Berrino *et al.* 1986) and taking advantage of numerical techniques (such as finite elements) which are able to handle the finite dimensions of the source and the characteristic features of the surrounding medium, such as stratification and the existence of the caldera (Bianchi *et al.* 1986). Although these models are able to reproduce the behaviour of the measured ground deformation as a function of the distance from the centre (which is also the point of maximum uplift), a very large pressure increase is required to produce an uplift of the order of those detected at Campi Flegrei. In fact, in order to obtain a vertical displacement of 1 m at the surface due to the presence of a point-like source at a depth $\xi = 3$ km, with an associated spehrical volume of radius $a = 1$ km, an instantaneous pressure increase of about 1 kbar is necessary, if the medium surrounding the source has a rigidity $\mu = 10^{11}$ dyne cm^{-2} and an incompressibility $K = 5/3\,\mu$ (from the formula given by Maruyama 1964). Such unreasonably high pressure increase would determine deviatoric stresses in the surrounding medium which are certainly beyond the yield strength of crustal rocks even if they were at ambient temperature (Griggs, Turner & Heard 1960). This shows that a model based on a centre of pressure (or dilation) embedded in an elastic medium (such as Mogi's model and those derived from it) cannot be applied to the study of ground deformation in volcanic areas like Campi Flegrei, where large uplifts occur.

In this paper, the viscoelastic pressure-source model is applied to Campi Flegrei with a pressure source history varying in time and the results for the ground uplift are discussed. The principal stresses and the maximum shear stress are derived for this model and related to the seismic activity at Campi Flegrei.

2 Elastic solution

Let us consider a homogeneous and isotropic elastic half-space with Lamé parameters and incompressibility $K = \lambda + \frac{2}{3}\mu$ (Fig. 3). The free surface is the plane $x_3 = 0$ and the x_3-axis penetrates into the elastic medium. We are looking for the static displacement field produced in the medium by a centre of dilation or pressure located at depth $x_3 = \xi$. It is well known (Steketee 1958; Maruyama 1964; Press 1965) that a point-like dislocation, including a centre of dilation, can be represented by a superposition of nine types of force couples which are characterized by two indices i and j ($i, j = 1, 2, 3$), where i denotes the direction of the forces and j denotes the direction of the couple arm (Fig. 4).

According to Maruyama (1964), the displacement field produced by a centre of dilation

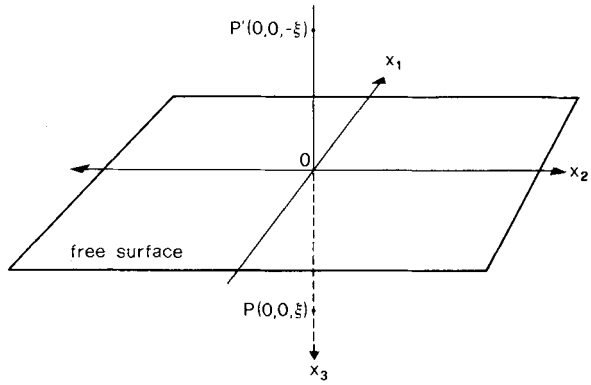

Figure 3. Viscoelastic half-space model. The centre of dilation or pressure is at depth $x_3 = \xi$.

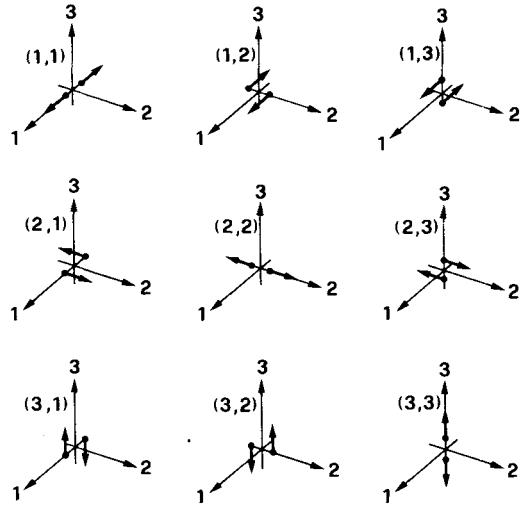

Figure 4. The nine couples of forces as defined in this paper.

will be obtained through the Galerkin vector, $\bar{\Gamma}$. This is defined as a vector from which the displacement field satisfying the equation of equilibrium is obtained according to:

$$u^k = \Gamma_k{}^{nn} - \alpha \Gamma_n{}^{nk} \tag{1}$$

where the displacement components are denoted by a superscript.

The quantity α is defined as:

$$\alpha = \frac{3K + \mu}{3K + 4\mu}. \tag{2}$$

The boundary conditions of the problem require that the plane $x_3 = 0$ is a free surface, i.e.

$$\sigma_{31} = \sigma_{32} = \sigma_{33} = 0; \qquad \text{at} \quad x_3 = 0 \tag{3}$$

where σ is the stress tensor. Moreover displacement and stress must vanish at infinity. The displacement field produced by a nucleus of strain in the elastic half-space can be obtained by superposition of three contributions: (1) the displacement produced by a nucleus at

point $(0, 0, +\xi)$ in an unbounded medium; (2) the displacement produced by an image nucleus at point $(0, 0, -\xi)$; (3) the displacement produced by a suitable distribution of normal forces on the plane $x_3 = 0$.

Let us call w^i_{kl} the contribution from the two nuclei at $x_3 = \xi$ and at $x_3 = -\xi$ to the i-component of displacement and ω^i_{kl} the analogous contribution from the force distribution on the plane $x_3 = 0$, the indices k and l denoting the type of nucleus.

The case $k = l$ corresponds to a centre of dilation (sum of three couples without moment) plus a couple without moment, while the case $k \neq l$ corresponds to a combination of two coplanar couples with moment. The case $k = l$ will be therefore considered in the following. Then, the displacement produced in the half-space can be written as:

$$u^i = m_0 g(t) \sum_{k,l} (w^i_{kl} + \omega^i_{kl}) \tag{4}$$

where m_0 is the intensity of the nucleus and $g(t)$ is its time history. If a volume V is associated with the nucleus, the intensity m_0 can be written as:

$$m_0 = V\Delta\Theta \tag{5}$$

in the case of a centre of dilation, where $\Delta\Theta$ is the fractional change in volume. A pressure change can also be associated with the centre of dilation, which represents the pressure variation necessary to produce a dilation $\Delta\Theta$ at the source.

If we want to calculate the displacement due to a pressure Δp_0 applied to the surface of a spherical cavity of volume V, the intensity m_0 must be rewritten as:

$$m_p = \frac{V\Delta P_0}{4\mu}. \tag{6}$$

According to (1) the displacements w^i_{kl} and $\omega^i{}_{kl}$ can be obtained from Galerkin vectors W^i_{kl} and Ω^i_{kl} respectively:

$$w^i_{kl} = W^i_{kl}{}^{,nn} - \alpha W^i_{kl}{}^{,ni} \tag{7}$$

$$\omega^i_{kl} = \Omega^i_{kl}{}^{,nn} - \alpha\Omega^i_{kl}{}^{,ni}. \tag{8}$$

Since the force distribution is normal to the plane $x_3 = 0$, the Galerkin vector $\bar{\Gamma}$ has only the third component different from zero. The expressions of W^i_{kl} and Ω^i_{kl} for a centre of dilation $(k = l)$ can be found in Maruyama (1964).

The displacement components w^i_{kk} and ω^i_{kk} calculated from (7) and (8) are given in Appendix A. Formulae (A1–A9) and (A19–A27) for the displacement field given in Appendix A differ from those given by Maruyama (1964) since they have been obtained for $\lambda \neq \mu$ and then rewritten in terms of K and μ.

For later use, we write here the expression for the vertical displacement $u^3(0)$ at the point $x_1 = x_2 = x_3 = 0$ derived from (4):

$$u^3(0) = m_{0,p}\, g(t) \frac{\beta - 4}{2\pi\xi^2} \tag{9}$$

where $\beta = 1/\alpha$.

3 Viscoelastic solution

For a linear viscoelastic material, the solution can be obtained from the elastic one employing the correspondence principle (e.g. Christensen 1971). One must replace the constants K

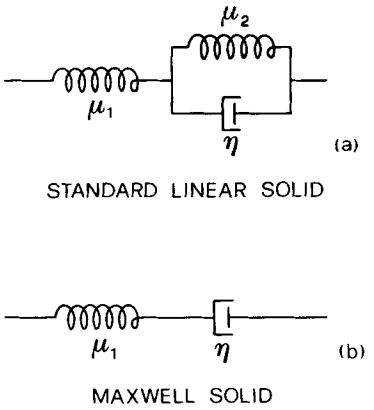

Figure 5. Mechanical models of the standard linear solid (SLS) (a) and the Maxwell solid (b).

and μ appearing in the elastic solution by their expressions as functions of the Laplace variable s, $\tilde{K}(s)$ and $\tilde{\mu}(s)$, which depend on the particular rheology considered. The source function $g(t)$ is substituted by its Laplace transform $\tilde{g}(s)$. In the case of a pressure source the intensity m_p must also be written as a function of s, $\tilde{m}_p(s)$, since it contains μ (*cf.* equation 6). The resulting expression is the Laplace transform of the viscoelastic solution. One must then invert it in order to obtain the solution in the time domain. Since most rocks flow to relax only shear stress, we shall replace only μ with $\tilde{\mu}(s)$, while K is left constant as in the elastic case. We assume that the rheology of the viscoelastic half-space is that of a standard linear solid (SLS) which is represented in Fig. 5a. In this case (see, e.g. Fung 1965):

$$\tilde{\mu}(s) = \frac{\mu_1 s + \mu_1 \mu_2/\eta}{s + (\mu_1 + \mu_2)/\eta} \tag{10}$$

where μ_1 and μ_2 are the rigidities and η is the viscosity. If $\mu_2 = 0$, the SLS reduces to the Maxwell solid (Fig. 5b). The Laplace transform of the displacement field produced by either the centre of dilation or the pressure source in the viscoelastic half-space is therefore:

$$\tilde{u}^i(s) = \tilde{m}_{0,p}(s)\,\tilde{g}(s) \sum_{k,l} [\tilde{w}^i_{kl}(s) + \tilde{\omega}^i_{kl}(s)] \tag{11}$$

where $\tilde{w}^i_{kl}$ and $\tilde{\omega}^i_{kl}$ are the expressions (A1–A9) and (A19–A27) respectively, in which the substitution $\mu \to \tilde{\mu}(s)$ has been made. The solution in the time domain can be written as:

$$u^i(\bar{x}, t) = \sum_{k,l} [\bar{w}^i_{kl}(\bar{x}, t) + \bar{\omega}^i_{kl}(\bar{x}, t)], \tag{12}$$

where

$$\bar{w}^i_{kl}(\bar{x}, t) = L^{-1}[\tilde{m}_{0,p}(s)\,\tilde{g}(s)\,\tilde{w}^i_{kl}(\bar{x}, s)] \tag{13}$$

and

$$\bar{\omega}^i_{kl}(\bar{x}, t) = L^{-1}[\tilde{m}_{0,p}(s)\,\tilde{g}(s)\,\tilde{\omega}^i_{kl}(\bar{x}, s)], \tag{14}$$

L^{-1} denoting Laplace inversion. The expression for the Laplace inversion of the displacement components w^i_{kl} and ω^i_{kl} are given in Appendix B.

We shall now employ a specific source function to model the time history of the centre of dilation or the pressure source in the viscoelastic half-space. We choose the Heaviside step function $H(t)$ for representing a change of volume or pressure at $t = 0$:

$$g(t) = H(t) = \begin{cases} 0; & t < 0 \\ 1; & t > 0 \end{cases}. \tag{15}$$

3.1 VISCOELASTIC SOLUTION FOR A CENTRE OF DILATION

For scaling the time, we choose the quantity:

$$\tau = \frac{(3K + \mu_1)\eta}{3K(\mu_1 + \mu_2) + \mu_1\mu_2}. \tag{16}$$

In order to estimate the effect of stress relaxation on the displacement at the Earth's surface, we calculate the ratio between the maximum vertical displacements at $x_3 = 0$ in the viscoelastic and in the elastic case, respectively. At each instant of time, the vertical displacement is maximum at $x_1 = x_2 = 0$. The elastic displacement coincides with the viscoelastic displacement at $t = 0$. Since the coefficients d in (B16) and (B17) are not positive, the viscoelastic displacement has a finite limit for $t \to \infty$, which is its maximum value in the time domain. If $u^3(\bar{x}, t)$ is the vertical displacement, we calculate therefore:

$$\frac{u^3(\bar{0}, \infty)}{u^3(\bar{0}, 0)} = \frac{(\mu_1 + \mu_2)(3K + \mu_1)}{\mu_1\mu_2 + 3K(\mu_1 + \mu_2)}. \tag{17}$$

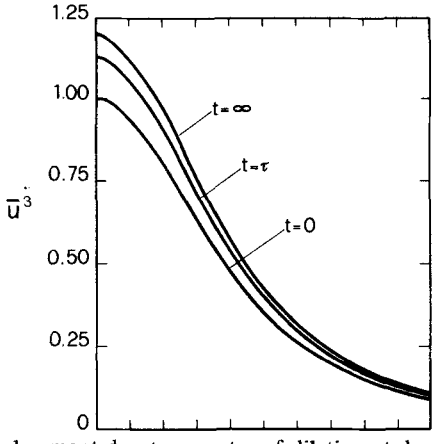

Figure 6. Vertical ground displacement due to a centre of dilation at depth $x_3 = \xi$, as a function of the radial distance r. The three curves refer to different times and are normalized to the maximum elastic displacement, which occurs at $r = 0$ and $t = 0$. Maxwell solid rheology.

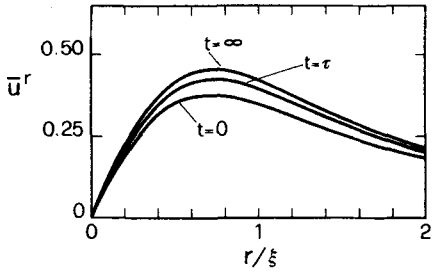

Figure 7. Horizontal ground displacement due to a centre of dilation. Details as in Fig. 6.

In the case of a Maxwell solid ($\mu_2 = 0$), if we assume moreover $K = {}^5/_3\mu_1$, the ratio (17) is equal to 1.2. Therefore, the ground deformation is amplified by 20 per cent as a consequence of viscoelasticity.

Figs 6 and 7 show respectively the vertical and the horizontal displacement at the Earth's surface as a function of r for a Maxwell rheology with $K = {}^5/_3\mu_1$, i.e. $\lambda = \mu_1$. The different curves refer to different times and displacements are normalized to the maximum vertical displacement at $t = 0$, i.e. the maximum elastic displacement. It can be seen that more than half of the viscoelastic effect occurs for $0 < t < \tau$.

In the case of the SLS rheology, with $\mu_1 = \mu_2$ and $K = {}^5/_3\mu_1$, the effect of viscoelasticity on the displacement at the Earth's surface is much less noticeable: the ratio between the vertical displacement at $t \to \infty$ and $t = 0$ is in fact about 1.09.

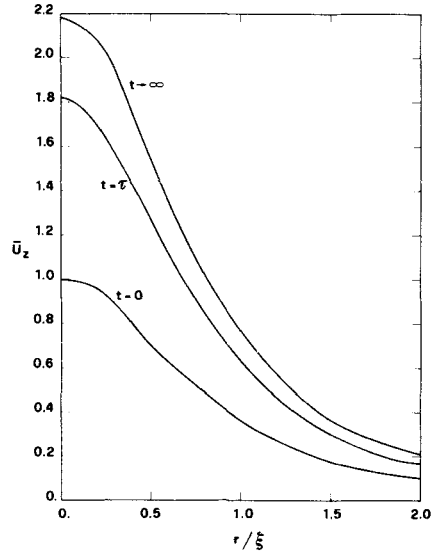

Figure 8. Vertical ground displacement due to a pressure source at depth $x_3 = \xi$. Details as in Fig. 6. Standard linear solid rheology.

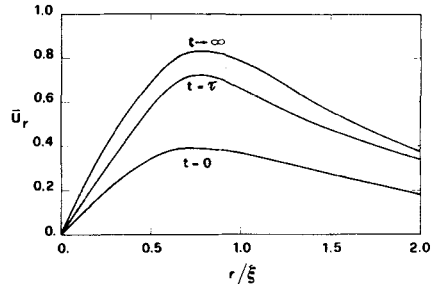

Figure 9. Horizontal ground displacement due to a pressure source at depth $x_3 = \xi$. Details as in Fig. 6. Standard linear solid rheology.

3.2 VISCOELASTIC SOLUTION FOR A CENTRE OF PRESSURE

For a centre of pressure embedded in a medium with SLS rheology, for which the Laplace inverse (B1), (B2), (B3) and (B4) have the form of (B17) (see Appendix B), the viscoelastic displacement has a finite limit for $t \to \infty$. The ratio between the limit for $t \to \infty$ and the elastic value of the vertical displacement at $x_1 = x_2 = 0$ is given by:

$$\frac{u^3(\bar{0}, t \to \infty)}{u^3(\bar{0}, 0)} = \frac{(3K + \mu_1)(\mu_1 + \mu_2)}{[3K(\mu_1 + \mu_2) + \mu_1\mu_2]\mu_2}. \tag{18}$$

If we assume $K = {}^5/_3\,\mu_1$ (i.e. $\lambda = \mu_1$) and $\mu_1 = \mu_2$, the ratio (18) is equal to about 2.2, which indicates that the ground deformation is amplified by a factor of about 2 due to viscoelasticity. Figs 8 and 9 show the vertical and the horizontal displacement at the surface, $x_3 = 0$, with $K = {}^5/_3\,\mu_1$ and $\mu_1 = \mu_2$, at $t = 0$, $t = \tau$ and $t \to \infty$. Although the amplification of the deformation is larger, the qualitative behaviour is very similar to the case of the centre of dilation.

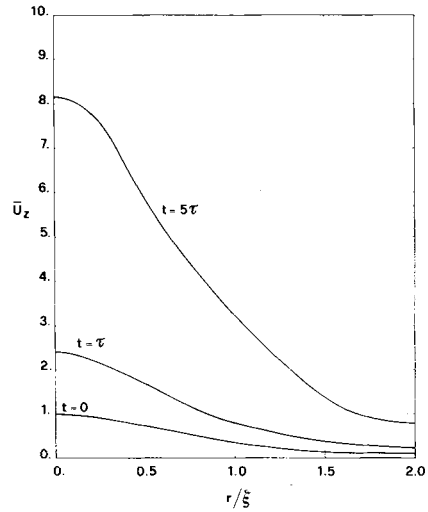

Figure 10. Vertical ground displacement due to a pressure source at depth $x_3 = \xi$. Details as in Fig. 6. Maxwell solid rheology.

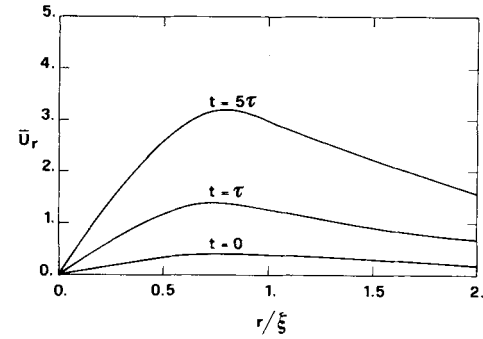

Figure 11. Horizontal ground displacement due to a pressure source at depth $x_3 = \xi$. Details as in Fig. 6. Maxwell solid rheology.

On the other hand, for a Maxwell solid rheology, due to the form of Laplace inverts (see B19), the displacement does not have a finite limit for $t \to \infty$, owing to the presence of a term proportional to the time t. Figs 10 and 11 show the horizontal and vertical displacements, with $K = {}^5/_3\,\mu_1$, at the surface $x_3 = 0$, for three values of time, $t = 0, \tau$ and 5τ.

4 Stress fields

Stress fields are now evaluated for the cases discussed in the previous section. The stress-strain relation in the Laplace variable domain reads:

$$\sigma_{ij} = K\delta_{ij}u_{n,n} + \mu(u_{i,j} + u_{j,i} - {}^2/_3\,\delta_{ij}u_{n,n}). \tag{19}$$

The stress as a function of time is given by the inversion of (19). The derivatives are taken numerically using a four-point, fourth-order accurate central formula (Ferziger 1981).

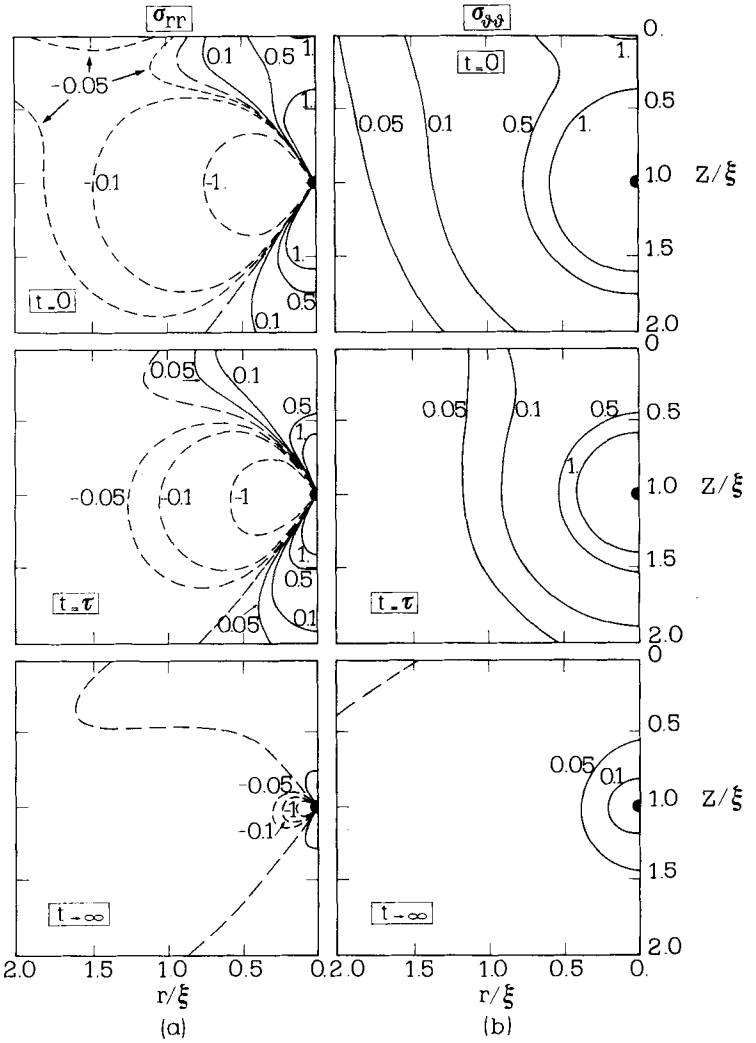

Figure 12. [*overleaf for (c), (d), (e)*] Stress field components due to a centre of dilation at depth $x_3 = \xi$ at three different times. Stress values are expressed in units of $\mu_1/100$. Solid lines denote positive values, dashed lines denote negative values. Maxwell solid rheology. (a) σ_{rr}, (b) $\sigma_{\vartheta\vartheta}$, (c) σ_{zz}, (d) σ_{rz}, (e) trace σ_{ii}.

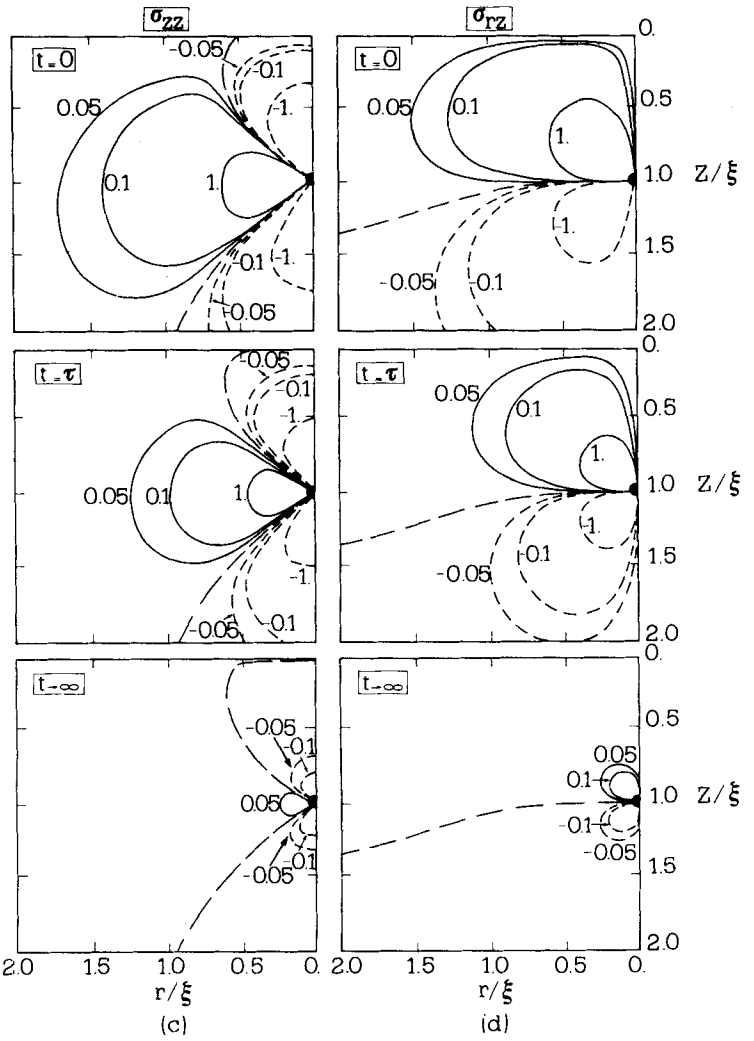

Figure 12 – *continued*

Since the geometry of the problem has a cylindrical symmetry, the components of the stress field are given as functions of the cylindrical coordinates z, r and ϑ defined as:

$$x_1 = r \cos \vartheta \tag{20a}$$

$$x_2 = r \sin \vartheta \tag{20b}$$

$$x_3 = z. \tag{20c}$$

Maps of stress components σ_{rr}, $\sigma_{\vartheta\vartheta}$, σ_{zz} and σ_{rz} due to a centre of dilation with the rheology of a Maxwell solid are shown in Fig. 12(a–d) respectively. In Fig. 12(e), the trace σ_{ii} of the stress field is shown.

The upper edge of each graph represents the Earth's surface, while the dot is the centre of dilation. For each stress component, three maps are shown, which are relative to different times. In all cases, the first map refers to $t = 0$ and therefore represents the elastic solution.

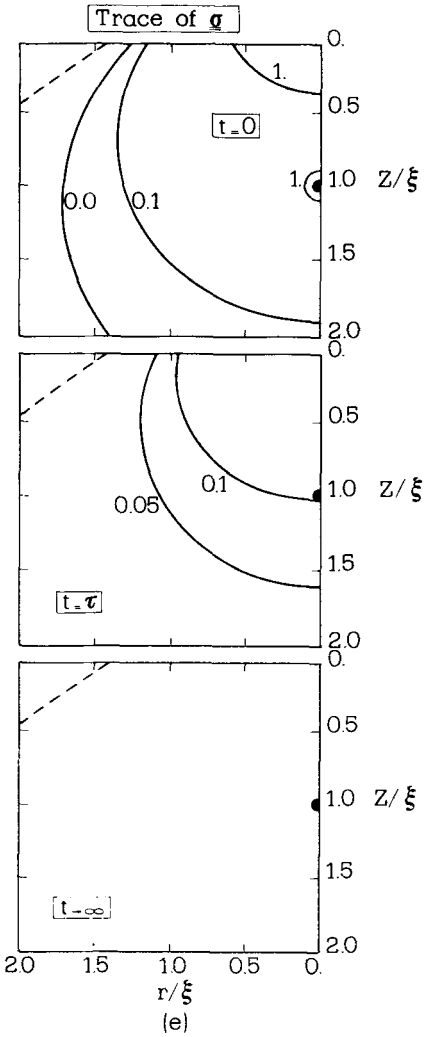

Figure 12 – *continued*

Stress relaxation is evident from the subsequent maps at $t > 0$. The last map for each component represents the permanent state of stress which is left in the medium as $t \to \infty$. This state of stress is virtually reached for $t = 5\tau$: further stress relaxation is negligible.

Fig. 13(a–e) shows respectively the stress components σ_{rr}, $\sigma_{\vartheta\vartheta}$, σ_{zz}, σ_{rz} and the trace σ_{ii} for a pressure source with the Maxwell rheology. In this case, stress relaxation is faster if expressed in units of τ: only two maps for each component are shown, since stress attains its asymptotic value already at $t = \tau$.

5 Application to volcanic areas

The presence of incoherent materials, such as volcanic products, and high temperatures typical of volcanic areas produces effective viscosities orders of magnitude lower than the characteristic values of the 'cold' Earth's crust, thus prompting one to take into account

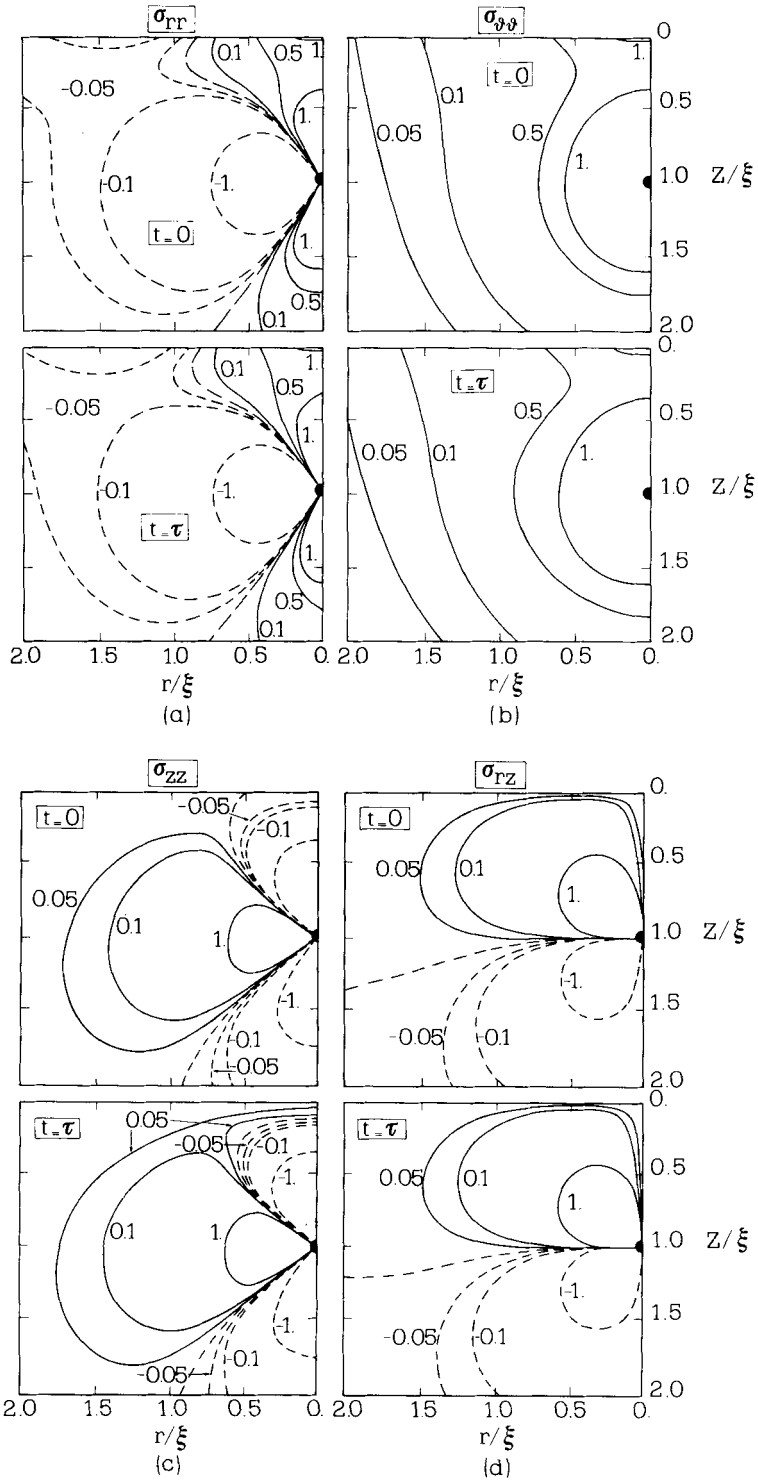

Figure 13. Stress field components due to a pressure source located at depth $x_3 = \xi$ at three different times. Stress values are expressed in units of $\mu_1/100$. Solid lines denote positive values, dashed lines denote negative values. Maxwell solid rheology. (a) σ_{rr}, (b) $\sigma_{\vartheta\vartheta}$, (c) σ_{zz}, (d) σ_{rz}, (e) trace σ_{ii}.

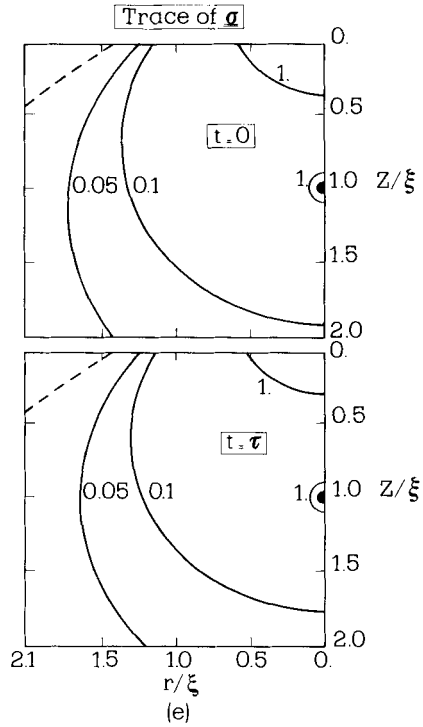

Figure 13 – *continued*

viscoelastic effects. For instance, in Campi Flegrei the temperature is over 300°C at 1 km depth, in the Mofete area, close to the rim of the cladera (Cioppi *et al.* 1980).

The pressure source model applies directly to the study of ground deformation in volcanic areas due to the presence of an insulated magma chamber where mechanisms of magma migration can provide a pressure increase on the surface of the chamber. We take as an example the volcanic area of Campi Flegrei, near Naples, Italy. In this region, two major ground deformation episodes occurred in the last 15 years and had a similar evolution. The first one began in 1970 and culminated in 1972 with a total uplift of about 60 cm, followed by a deflation of about 20 cm till the end of 1973. The second one started in 1982 and ended about two years later, producing a total uplift of 160 cm (Berrino *et al.* 1986) followed by a deflation at the rate of about 1 mm day^{-1} (Berrino *et al.*, note presented at the 'Riunione Scientifica sui Campi Flegrei', Naples, 1985 March 28). In Fig. 1 the ground uplift in the town of Pozzuoli (see map in Fig. 19) is shown from 1970 to 1986, while in Fig. 2b it is plotted against the distance from Pozzuoli (which is the point where the maximum uplift has been measured) at three different times.

The model employed in this paper to represent Campi Flegrei is sketched in Fig. 14 where a spherical cavity of radius a, representing the magma chamber, is associated with the point-like source located at a depth ξ. The medium surrounding the magma chamber has a Maxwell solid rheology: this choice is due to the great uncertainty affecting our knowledge of the two rigidity values appearing in the SLS rheology. A pressure $\Delta p_0 g(t)$ is applied to the spherical cavity surface and is responsible for the deformations in the medium. For the application to the Campi Flegrei, on the basis of geological evidence (Armienti *et al.* 1983; Berrino *et al.* 1986) we take a = 1 km and ξ = 3 km. The temporal behaviour of the applied

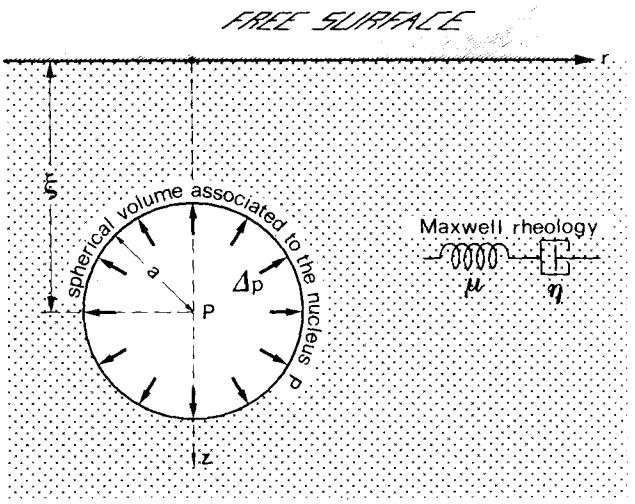

Figure 14. Sketch of the viscoelastic pressure source model applied to the study of a volcanic site. A spherical magma chamber of radius a is buried at depth ξ in a medium endowed with a Maxwell rheology and a pressure $\Delta p\,(t)$ is applied to the surface of the spherical cavity.

pressure will be discussed and a source history will be chosen such that the produced ground uplift is in agreement with observations.

However, the purpose of this paper is not the discussion of the magmatic processes which can produce the source history chosen, neither a close fit of the measured data, but the understanding of the mechanics of the deformation process. A quantitative fit of data will be possible only with a more realistic model which takes into account the stratification of the medium and viscosity variations.

The results obtained in the case of a pressure suddenly applied to the surface of a spherical cavity, show that viscoelasticity plays a fundamental role. In fact, by virtue of viscoelasticity, the final displacements are amplified with respect to the initial elastic ones by about 120 per cent in the case of a pressure source with SLS rheology. Furthermore, the results are interesting in the case of a pressure source located in a medium characterized by a Maxwell solid rheology. In this case, for a sudden application of pressure, the vertical displacement at the surface grows indefinitely in time, at a rate which approaches a constant value, after a transient phase. The characteristic time of the process is:

$$\tau = \frac{(3K + \mu_1)\eta}{3K\mu_1}. \tag{21}$$

For $t \gg \tau$, the uplift rate is given by:

$$\left| \frac{du^3}{dt} \right| = \frac{3V\Delta p_0}{8\pi\xi^2\eta} \tag{22}$$

where u^3 is the ground uplift and V is the spherical volume (of radius a) associated with the point-like source. The quantity $V\Delta p_0$ has not necessarily to be considered as a volume times a pressure variation, but in a more general scheme, it represents an adiabatic variation of enthalpy. From (22), if the source has a radius $a = 1$ km and is located at a depth $\xi = 3$ km and a Δp_0 value of about 60 bar applied to the magma chamber surface, a viscosity $\eta = 10^{17}$

poise is required in the surrounding medium to produce an uplift rate of 1 m yr^{-1}, i.e. of the order of the uplift rate measured at Campi Flegrei (Berrino *et al.* 1986). Furthermore, for $\mu_1 = 5 \times 10^{10}$ dyne cm^{-2} (as seismic data suggest), $K = \frac{5}{3}\mu_1$, the characteristic time of the process is about 1 month, which compares favourably with the two months time lag between the drop of the geochemical anomalies detected at Campi Flegrei and the end of the uplift movement in late 1984 (Carapezza *et al.*, note presented at the 'Riunione Scientifica sui Campi Flegrei', Naples, 1985 March 28).

In this model, the stress components have a finite limit which does not differ considerably from the elastic value for the same Δp_0, thus being in agreement with the nearly continuous seismicity that occurred at Campi Flegrei during the uplift process.

In order to get a more realistic picture, in the present paper the convolution of the Green's functions with a different source history $g(t)$ is performed. The source history chosen has a trapezoidal shape, since it increases linearly in time from 0 to 1 for t ranging between 0 and t_1, remains then constant, equal to 1, for $t_1 \leqslant t \leqslant t_2$, and finally decreases to 0, for $t_2 \leqslant t \leqslant t_3$:

$$g(t) = \frac{t}{t_1}[1 - H(t - t_1)] + H(t - t_1) - H(t - t_2) + \frac{t_3 - t}{t_3 - t_2}[H(t - t_2) - H(t - t_3)]. \quad (23)$$

The time-dependent vertical displacement $u^3(r, z, t)$ obtained by the convolution of the appropriate Green's function with the trapezoidal source history takes the following form:

$$u^3(r, z, t) = \frac{1}{t_1}[u^3_L(r, z, t) - H(t - t_1)\, u^3_L(r, z, t - t_1)]$$

$$- \frac{1}{t_3 - t_2}[H(t - t_2) u^3_L(r, z, t - t_2) - H(t - t_3) u^3_L(r, z, t - t_3)] \quad (24)$$

where $u^3_L(r, z, t)$ is the result of the convolution of the Green's function for the vertical displacement with a source history $g(t) = t$ increasing linearly with time. At the surface $z = 0$ and at $r = 0$, $u^3_L(0, 0, t)$ takes the following form:

$$u^3_L(0, 0, t) = \frac{V\Delta p_0}{8\mu_1 \mu \xi^2}\eta\left\{\frac{\mu_1}{3K^2}(e^{-t/\tau} - 1)\frac{(3K + \mu_1)(\mu_1 - 3K)}{3K^2\mu_1}\frac{t}{\tau} - \frac{(3K + \mu_1)^2}{6\mu_1 K^2}\left(\frac{t}{\tau}\right)^2\right\}. \quad (25)$$

The surface uplift at $r = 0$ is obtained by substituting (25) in (24) and the solution depends on the choice of t_1, t_2, t_3, which determine the source history, and $m_{0,p}$, which measures the source intensity or, once the volume is fixed, the pressure applied to its surface.

5.1 GROUND DEFORMATIONS

In order to choose properly the values of the four unknown parameters t_1, t_2, t_3 and Δp_0, assuming that the radius of the source and its depth are known together with the rheological constants μ_1, K and η, a more careful analysis is necessary.

A simple expression of the uplift at $r = 0$ for $t \gg t_3$, which gives the value of the ground level after the deformation process is over, can be written, taking the asymptotic expression of (24) and (25):

$$u^3(t \gg t_3) = \frac{3V\Delta p_0}{16\pi\xi^2\eta}(t_1 - t_2 - t_3). \quad (26)$$

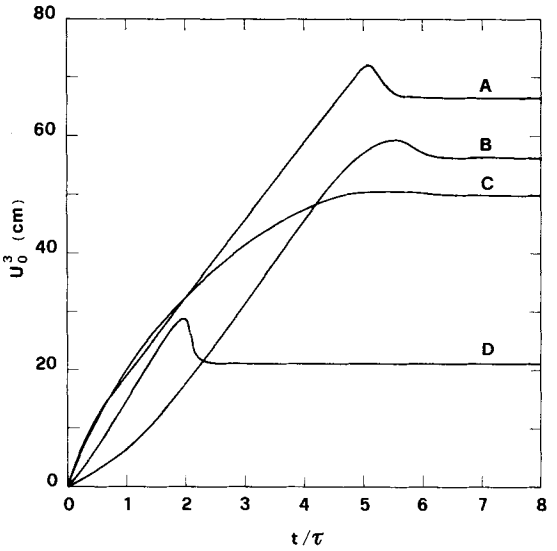

Figure 15. Ground uplift as a function of time obtained from the viscoelastic pressure source model. Trapezoidal source histories are employed with $t_1 = \tau/2$, $t_2 = 5\tau$ and $t_3 = 5.5\tau$ (curve A); $t_1 = 2.5\,\tau$, $t_2 = 5\tau$ and $t_3 = 6\tau$ (curve B); $t_1 = \tau/2$, $t_2 = 2\tau$ and $t_3 = 6\tau$ (curve C); $t_1 = \tau$, $t_2 = 2\tau$ and $t_3 = 2.2\tau$ (curve D). The radius of the source, located at a depth of 3 km, is 1 km. The rheological parameters for the surrounding medium are $\mu_1 = 5 \times 10^{10}$ dyne cm^{-2}, $K = {}^5/_3\,\mu_1$, $\eta = 10^{17}$ P. The applied pressures is 100 bar.

Fig. 15 shows four curves representing the ground uplift as a function of time obtained with $\mu_1 = 5 \times 10^{10}$ dyne cm^{-2}, $K = {}^5/_3\,\mu_1$, $\eta = 10^{17}$ poise, $\Delta p_0 = 100$ bar (the radius of the source is equal to 1 km), but with different choices of the time values which characterize the source history. Curve (A) is obtained with $t_1 = \tau/2$, $t_2 = 5\tau$ and $t_3 = 5.5\tau$; curve (B) has $t_1 = 2.5\tau$, $t_2 = 5\tau$ and $t_3 = 6\tau$; curve (C) has $t_1 = \tau/2$, $t_2 = 2\tau$ and $t_3 = 6\tau$; curve (D) has $t_1 = \tau$, $t_2 = 2\tau$ and $t_3 = 2.2\tau$. The first thing to be noted is that the peak representing the maximum uplift is sharper if t_3 is close to t_2, as in curves (A) and (D). The deflation, in this case, is more pronounced, being about 10 and 30 per cent in curves (A) and (D), respectively, and only about 6 and 2 per cent in curves (B) and (C). Curve (B) also exhibits a very slow initial gradient, due to the fact that the pressure applied at the source increases with $t_1 = 2.5$.

The maximum value of the uplift also depends on the combination of t_1, t_2 and t_3, once $V\Delta p_0$ and the depth of the source are fixed. Among the four cases taken as examples in Fig. 15, the smallest uplift is given by curve (D) which has the lowest value of t_2: the vertical displacement does not have the time to grow as in the other cases, since the pressure at the source begins to decrease after only 2τ. Curve (A) exhibits the highest maximum uplift, since the time t_2, during which the applied pressure increases or remains constant, is the longest, 5τ. Curves (B) and (A) have the same t_2, but the pressure increase is slower for curve (B), since $t_1 = 2.5\tau$, thus allowing a smaller uplift.

For $t_1 = \tau$, $t_2 = 2.5\tau$, $t_3 = 3.5\tau$ and $\Delta p_0 = 100$ bar a value of 33 cm is obtained from (26), which is of the same order as the permanent ground deformation shown in Fig. 1. Fig. 16 shows the plot of the theoretical curve obtained choosing the parameters t_1, t_2 and t_3 equal to τ, 2.5τ, 3.5τ respectively. The theoretical curve is very similar to the trend of the uplift data (Fig. 1), showing an inflation at a nearly constant strain rate which culminates with a

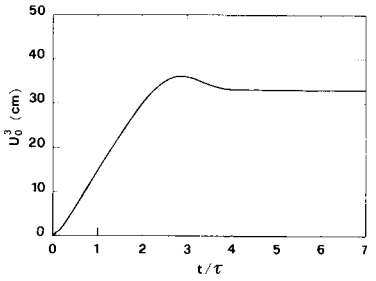

Figure 16. Ground uplift as a function of time obtained from the viscoelastic pressure source model and a trapezoidal source history with $t_1 = \tau$, $t_2 = 2.5\tau$ and $t_3 = 3.5\tau$.

maximum and, then, a deflation after which the ground level remains constant. Furthermore, with this choice for the parameters, a maximum uplift of about 35 cm occurs with the application of a pressure of only 100 bar at the source. This value constitutes a much more reasonable estimate than the one obtained from whichever kind of Mogi's model.

5.2 SEISMIC ACTIVITY

From the solutions obtained for displacement in the viscoelastic pressure-source model, the stress field can be derived and from the analysis of the maximum shear stress information on seismic activity can be achieved.

In this section a trapezoidal source history is employed with $t_1 = \tau$, $t_2 = 2.5\tau$ and $t_3 = 3.5\tau$.

First, we suppose that fracture can start in the medium if the maximum shear stress, σ_M, is larger than the strength, σ_y. The value of the strength depends upon the material itself and its temperature and pressure. The determination of in field rock strength values is still an open question in seismology. The study of earthquakes allows one to estimate the stress drops produced (typically in the range between 1 and 100 bar), although it does not give any piece of information on the absolute values of the initial and final stresses. Laboratory experiments on rock specimens suggest strength values much higher than 100 bar. However, *in situ* conditions (pore pressure, fault gauge) should possibly decrease the values measured in the experiments (e.g. Kanamori 1980). We assume here that rock strength is constant, equal to 20 bar.

Fig. 17(a–d) shows a vertical section of the viscoelastic half-space in which the magma chamber is embedded (shaded area); r denotes the distance from the surface point above the centre of the magma chamber and z the depth. In the figure the isolines of the maximum shear stress σ_M are drawn at different times $t = \tau/3$, $\tau/2$, $3\tau/2$ and $5\tau/2$. The hatched area shows the region where the maximum shear stress is larger than the strength and earthquakes can occur. It is noteworthy that, since $t = \tau/3$, there exists a region – though of limited size – within which seismic events may originate: this region grows with the pressure applied to the magma chamber surface. The maximum distance from the centre to which the seismogenic region expands is of the same order as the depth of the magma chamber, as shown in Fig. 17c. When the pressure applied to the magma chamber begins to decrease, also the stress values in the surrounding medium become lower and the region where $\sigma_M \geq \sigma_y$ contracts. In Fig. 17(d) we observe that, at $t = {}^5/_2\,\tau$, the maximum shear stress exceeds σ_y only in a restricted region around the magma chamber. Since in our stress calculations we

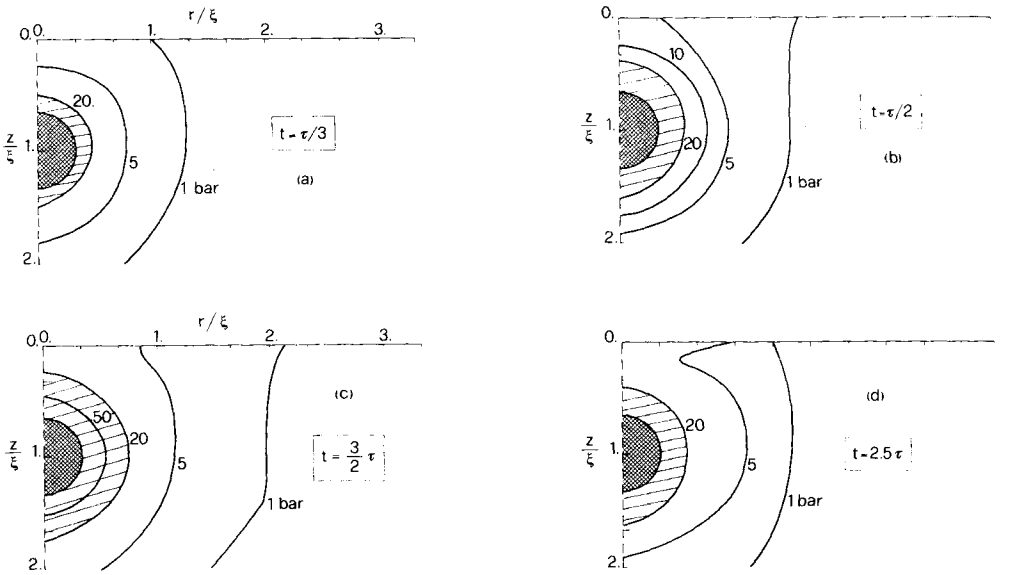

Figure 17. Isolines of maximum shear stress σ_M in the medium surrounding the magma chamber (dashed half circle) at $t = \tau/3$ (a), $t = \tau/2$ (b), $t = 3/2\,\tau$ (c), and $t = 5/2\,\tau$ (d), obtained from the viscoelastic pressure source model with a trapezoidal source history (*cf.* Fig. 16). The hatched areas represent the regions where σ_M is larger than a fixed yield strength $\sigma_y = 20$ bar, i.e. the seismogenic regions.

did not subtract the stress drop from the earthquakes which occurred during the inflation of the volcanic area, the hatched area in Fig. 17d is possibly larger than the actual seismogenic region. Then, we can reasonably assess that volcanic areas can be seismically active during the high rate ground uplift phase and that seismic activity stops after the uplift rate starts decreasing. Furthermore, the region interested by seismicity extends at most to a distance of a few kilometres from the central point.

In Fig. 18(a, b) we show principal deviatoric stresses in the medium surrounding the magma chamber, at $t = \tau/2$, i.e. while the applied pressure increases, and $t = {}^3/_2\,\tau$, i.e. while the applied pressure remains constant. In the figure two components of the principal deviatoric stress are shown with their orientations; the third component is normal to the figure plane and its absolute value is lower than or intermediate between that of the two others. First, we note that stress orientations, and so the earthquake mechanism distribution, do not change in time. For this reason, one can expect that during all the time when the area is seismically active, normal earthquakes (vertical principal stress maximum) occur in the central region, within a distance of the order of the magma chamber radius, and that compressive earthquakes occur elsewhere.

On the basis of our calculations, we then conclude that the seismogenic zone in Campi Flegrei extends at a distance of about 2.5 km from the town of Pozzuoli, which is the point where the maximum uplift has been measured (shaded and dotted areas in Fig. 19). Within this seismically active area, two distinct regions can be recognized, depending on the earthquake mechanism type. In fact, within a distance of about 1.5 km from Pozzuoli, normal earthquakes occur, being this zone characterized by a maximum principal stress aligned along the vertical axis (shaded area in Fig. 19). On the other hand, in the outer part of the seismogenic region, from a distance of about 1.5 to about 2.5 km from Pozzuoli, one expects compressive mechanisms for earthquakes (dotted area in Fig. 19). From the maximum shear

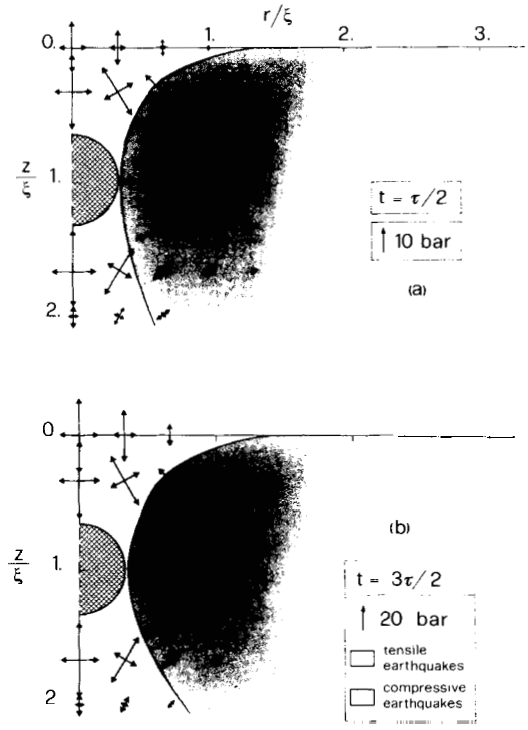

Figure 18. Principal deviatoric stress field in the medium surrounding the magma chamber (shaded half circle) obtained from the viscoelastic centre of pressure model with a trapezoidal source history (*cf.* Fig. 16). The lighter area represents the region where compressive earthquakes can occur; the darker area is the region where tensile earthquakes must be expected.

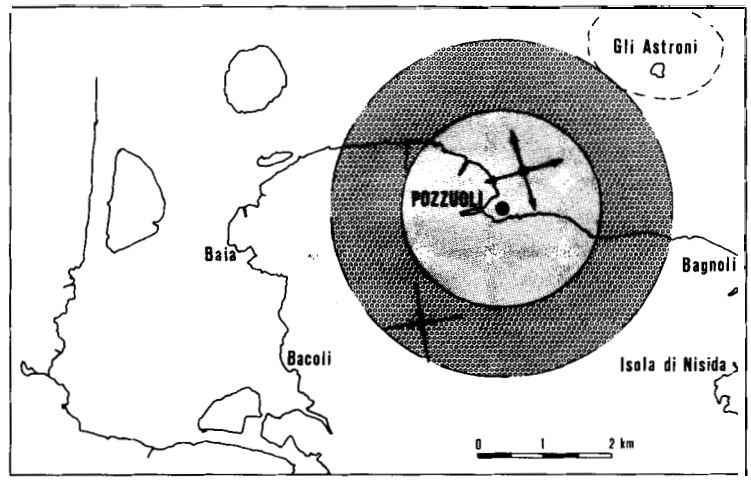

Figure 19. Map of the Campi Flegrei, Italy. The two shaded areas around the town of Pozzuoli represent the region where seismic event can be expected, on the basis of our model: in the inner area compressive earthquakes can occur, while in the outer area tensile earthquakes must be expected.

eruption. Thus, both models are inadequate to represent the deformation in volcanic areas, although the introduction of viscoelasticity helps obtaining less unreasonable values for the pressure change responsible for the ground displacements.

On the other hand, in the pressure source model with a Maxwell solid rheology, the behaviour of the solution is different. In fact, the viscoelastic displacement has no finite limit for $t \to \infty$, but grows indefinitely in time. The geophysical observable which has to be explained by such a model is, then, the uplift rate, rather than the total uplift. The expression of the viscoelastic ground uplift, at $x_1 = x_2 = x_3 = 0$ reads (*cf.* 9):

$$u^3(0) = \frac{V\Delta p_0}{8\pi\mu_1\xi^2}\,[\beta(t) - 4g_1(t)]. \tag{27}$$

Differentiation of (27) with respect to t, with the substitution of the explicit expressions for $\beta(t)$ and $g_1(t)$, gives the uplift rate:

$$\frac{du^3}{dt} = -\frac{3V\Delta p_0}{8\pi\xi^2\eta}\left\{\frac{3\mu_1^2}{(3K+\mu_1)^2}\exp(-t/\tau) - 1\right\}. \tag{28}$$

After a transient phase, the uplift rate approaches the constant value:

$$\left|\frac{du^3}{dt}\right| = \frac{3V\Delta p_0}{8\pi\xi^2\eta}. \tag{29}$$

A 1 m uplift which occurs in a time 15τ at the rate given by (29), requires a pressure change Δp_0 of only 100 bar, which is compared favourably with petrological estimates of pressure released by differentiation of trachybasalts.

With the introduction of viscoelasticity the required value of the pressure applied to the source surface is reduced by a factor of 10 or more, so that only a few tens of bars may be enough to produce the uplift. Furthermore, the behaviour of the ground level as a function of time is reproduced in a qualitative way by using a trapezoidal source history, as the comparison between Fig. 1 and Figs 15 and 16 shows.

The larger discrepancy between our theoretical profiles and the data is in the deflation phase. In fact, with this model the decrease of the ground level is fast and pronounced (as with curves A and D in Fig. 15) or slow but very small (as with curves B and C).

As concerns the seismicity, on the basis of the results obtained with our model with a trapezoidal source history, one can assess that seismic activity can only start after the source pressure generates deviatoric stresses higher than a threshold for brittle fracture and should stop when the uplift rate decreases. Assuming a yield strength of 20 bar, the seismogenic zone extends at most to a distance of the order of the magma chamber depth from the maximum uplift point, i.e. about 3 km from the town of Pozzuoli in the case of Campi Flegrei. Furthermore, the study of seismic mechanisms from the analysis of principal stresses allows one to expect normal fault mechanisms within a distance of the order of the magma chamber radius and compressive mechanisms in the outer part of the seismogenic zone (see Fig. 19) as observed (De Natale & Zollo 1985). An interesting feature of our model is that the region where deviatoric stresses are in excess of rock strength has nearly constant extension during the uplift phase, while in a purely elastic medium its extension would steadily increase with time, leading to an outward migration of seismic activity which is not observed.

Another mechanism has been suggested to explain ground deformation and seismicity at Campi Flegrei, which ascribes the inflation to a variation of pore pressure due to convective motion in an aquifer (Oliveri del Castillo & Montagna 1984). However, it is very hard to

explain in this way an axysimmetric uplift as observed at Campi Flegrei; furthermore, as time elapses, pore-fluid diffusion would increase the width of the uplift profile, which is not observed (Fig. 2), and seismic activity should also migrate outward.

Although the model presented here cannot pretend to reproduce exactly the dynamics of Campi Flegrei since many simplifying assumptions have been made (the most crucial being the assumption of homogeneity), it solves a number of issues such as the pressure required to produce large uplifts, the relation between stress and strain in the area and, furthermore, describes approximately the gross features of the inflation episodes, such as the *nearly constant uplift rate* of the central uplift and the final *deflation episode.* Furthermore the predicted seismicity is in good agreement with the observations made during the last uplift episode. It is clear that it would be extremely premature at this time to pretend to fit quantitatively the data by the present model. However, since we believe that the mechanics of the problem has been understood in principle, several questions can be now addressed quantitatively resorting to numerical techniques: more realistic source models can be devised in which all the available geophysical and geological information can be included.

Acknowledgments

The authors wish to thank F. Barberi, E. Boschi and F. Innocenti for the suggestions, comments and discussions which helped their work. Mr M. Bacchetti drew the figures. The research was performed with the contribution of the Gruppo Nazionale per la Vulcanologia, CNR.

References

Armienti, P., Barberi, F., Bizouard, H., Clocchiatti, R., Innocenti, F., Metrich, N., Rosi, M. & Sbrana, A., 1983. The Phlegraean Fields: magma evolution within a shallow chamber, *J. Volcanol. Geotherm. Res.*, **17**, 289–311.

Ben-Menahem, A. & Gillon, A., 1970. Crustal deformation by earthquakes and explosions, *Bull. seism. Soc. Am.*, **60**, 193–215.

Berrino, G., Corrado, G., Luongo, G. & Toro, B., 1986. Ground deformations and gravity changes accompanying the 1982 Pozzuoli uplift, *Bull. Volcanol.*, in press.

Bianchi, R., Coradini, A., Federico, C., Giberti, G., Sartoris, G. & Scandone, R., 1986. Modelling of surface ground deformations in the Phlegraean fields volcanic area, Italy, *Bull. Volcanol.*, in press.

Christensen, R. M., 1971. *Theory of Viscoelasticity: an Introduction,* Academic Press, New York.

Cioppi, D., Ghelardoni, R., Panci, G., Sommaruga, C. & Verdiani, G., 1980. *Demonstration project: evaluation of the Mofete high enthalpy reservoir (Phlegraean Fields),* note presented at the Second International Seminar of the Commission of European Communities, Strasbourg, France.

Corrado, G., Guerra, I., Lo Bascio, A., Luongo, G. & Rampoldi, R., 1976. Inflation and microearthquake activity of Phlegraean Fields, Italy, *Bull. Volcanol.*, **40**, 169–188.

De Natale, G. & Zollo, A., 1985. Parametri di sorgente e caratteristiche del mezzo di propagazione ai Campi Flegrei dedotti dall'analisi di dati da una rete digitale a 3 componenti, in *Proc. I Workshop on 'Aree sismogenetiche e rischio sismico in Italia'*, ed. Boschi, E., in press.

Dieterich, J. H. & Decker, R. W., 1975. Finite element-modelling of surface deformation associated with volcanism, *J. geophys. Res.*, **80**, 4094–4102.

Ferziger, J. H., 1981. *Numerical Methods for Engineering Applications,* p. 54, Wiley, New York.

Fiske, R. S. & Kinoshita, W. T., 1969. Inflation of Kilauea volcan prior to its 1967–1968 eruption, *Science*, **165**, 341–349.

Fung, Y. C., 1965. *Foundations of Solid Mechanics,* Prentice-Hall, Englewood Cliffs.

Griggs, D. T., Turner, F. J. & Heard, H. C., 1960. Deformation of rocks at 500 to 800C, in *Rock Deformation, Mem. geol. Soc. Am.*, **79**, 39–104.

Kanamori, H., 1980. The state of stress in the Earth's lithosphere, in *Physics of the Earth's Interior*, eds Dziewonski, A. M. & Boschi, E., *Proc. int. School of Physics 'Enrico Fermi'*, North Holland, Amsterdam.

Love, A. E. H., 1927. *A Treatise on the Mathematical Theory of Elasticity*, Dover, New York.

Maruyama, T., 1964. Statical elastic dislocations in an infinite and semi-infinite medium, *Bull. Earthq. Res. Inst. Tokyo Univ.*, **42**, 289–368.

Mindlin, R. D. & Cheng, D. H., 1950. Nuclei of strain in the semi-infinite solid, *J. appl. Phys.*, **21**, 926–930.

Mogi, K., 1958. Relations of the eruptions of various volcanoes and the deformations of the ground surface around them, *Bull. Earthq. Res. Inst. Tokyo Univ.*, **36**, 99–134.

Oliveri del Castillo, A. & Montagna, S., 1984. *Nuovi elementi sulla connessione tra termofluidodinamica e geodinamica ai Campi Flegrei (Napoli) – Bradisismo 1982–1984*, note presented at the 'Convegno annuale di Geofisica della Litosfera', Rome. Italy.

Palumbo, A., 1985. Influence of external tidal and meteorological forces on the bradyseismic phenomenon in the Phlegraean Fields, *Il Nuovo Cimento*, **8C**, 538–551.

Press, F., 1985. Displacements, strains and tilts at teleseismic distances, *J. geophys. Res.*, **70**, 2395–2412.

Rundle, J. B., 1978a. Gravity changes and the Palmdale uplift, *Geophys. Res. Lett.*, **5**, 41–44.

Rundle, J. B., 1978b. Viscoelastic crustal deformation by finite quasi-static sources, *J. geophys. Res.*, **83**, 5937–5945.

Rundle, J. B. & Whitcomb, J. H., 1984. A model for deformation in Long Valley, California, 1980–1983, *J. geophys. Res.*, **89**, 9371–9380.

Rundle, J. B. *et al.*, 1985. Seismic imaging in Long Valley, California, by surface and borehold techniques: an investigation of active tectonics, *EOS Trans. Am. geophys. Un.*, **66**, 94–201.

Savage, J. C. & Clark, M. M., 1982. Magmatic resurgence in Long Valley Caldera, California: possible cause of the 1980 Mammoth Lakes earthquakes, *Science*, **217**, 531–533.

Singh, S. K. & Sabina, F. J., 1975. Epicentral deformation based on the dilatancy-fluid diffusion model, *Bull. seism. Soc. Am.*, **65**, 845–854.

Steketee, J. A., 1985. On Volterra's dislocations in a semi-infinite elastic medium, *Can. J. Phys.*, **36**, 192–205.

Walsh, J. B. & Decker, R. W., 1975. Surface deformation associated with volcanism, *J. geophys. Res.*, **76**, 3291–3302.

Appendix A

The displacement components w^i_{kI} are calculated from the Galerkin vectors given by Maruyama (1964) and following equation (7) in the text. They are given by:

$$w^1_{11} = \frac{1}{4\pi}\alpha_1\left(\frac{x_1}{R^3}+\frac{x_1}{S^3}\right)+\frac{3}{4\pi}\alpha\left(\frac{x_1^3}{R^5}+\frac{x_1^3}{S^5}\right) \tag{A1}$$

$$w^2_{11} = -\frac{1}{4\pi}\alpha_1\left(\frac{x_2}{R^3}+\frac{x_2}{S^3}\right)+\frac{3}{4\pi}\alpha\left(\frac{x_2x_1^2}{R^5}+\frac{x_2x_1^2}{S^5}\right) \tag{A2}$$

$$w^3_{11} = -\frac{1}{4\pi}\alpha_1\left(\frac{x_3-\xi}{R^3}+\frac{x_3+\xi}{S^3}\right)+\frac{3}{4\pi}\alpha\left(\frac{(x_3-\xi)x_1^2}{R^5}+\frac{(x_3+\xi)x_1^2}{S^5}\right) \tag{A3}$$

$$w^1_{22} = -\frac{1}{4\pi}\alpha_1\left(\frac{x_1}{R^3}+\frac{x_1}{S^3}\right)+\frac{3}{4\pi}\alpha\left(\frac{x_1x_2^2}{R^5}+\frac{x_1x_2^2}{S^5}\right) \tag{A4}$$

$$w^2_{22} = \frac{1}{4\pi}\alpha_1\left(\frac{x_2}{R^3}+\frac{x_2}{S^3}\right)+\frac{3}{4\pi}\alpha\left(\frac{x_2^3}{R^5}+\frac{x_2^3}{S^5}\right) \tag{A5}$$

$$w^3_{22} = -\frac{1}{4\pi}\alpha_1\left(\frac{x_3-\xi}{R^3}+\frac{x_3+\xi}{S^3}\right)+\frac{3}{4\pi}\alpha\left(\frac{(x_3-\xi)x_2^2}{R^5}+\frac{(x_3+\xi)x_2^2}{S^5}\right) \tag{A6}$$

$$w_{33}^1 = -\frac{1}{4\pi}\alpha_1\left(\frac{x_1}{R^3}+\frac{x_1}{S^3}\right)+\frac{3}{4\pi}\alpha\left(\frac{x_1(x_3-\xi)}{R^5}+\frac{x_1(x_3+\xi)}{S^5}\right) \tag{A7}$$

$$w_{33}^2 = -\frac{1}{4\pi}\alpha_1\left(\frac{x_2}{R^3}+\frac{x_2}{S^3}\right)+\frac{3}{4\pi}\alpha\left(\frac{x_2(x_3-\xi)}{R^5}+\frac{x_2(x_3+\xi)}{S^5}\right) \tag{A8}$$

$$w_{33}^3 = \frac{1}{4\pi}\alpha_1\left(\frac{x_3-\xi}{R^3}+\frac{x_3+\xi}{S^3}\right)+\frac{3}{4\pi}\alpha\left(\frac{(x_3-\xi)^3}{R^5}+\frac{(x_3+\xi)^3}{S^5}\right) \tag{A9}$$

where

$$p = x_3+\xi \tag{A10}$$

$$r = \sqrt{x_1^2+x_2^2} \tag{A11}$$

$$S = \sqrt{r^2+(x_3+\xi)^2} \tag{A12}$$

$$R = \sqrt{r^2+(x_3-\xi)^2} \tag{A13}$$

$$\beta = \frac{3K+4\mu}{3K+\mu} = \frac{1}{\alpha} \tag{A14}$$

$$\alpha_1 = \frac{3K+4\mu}{3\mu}. \tag{A15}$$

More shortly, the components w_{kk}^i can be written as:

$$w_{kk}^i = \alpha_1 Q_{kk}^i + \alpha P_{kk}^i \tag{A16}$$

where

$$Q_{kk}^i = \frac{1}{4\pi}(-1)^{\delta ki+1}\left(\frac{x_i-\xi_i}{R^3}+\frac{x_i+\xi_i}{S^3}\right) \tag{A17}$$

$$P_{kk}^i = \frac{3}{4\pi}\left(\frac{(x_i-\xi_i)(x_k-\xi_k)}{R^5}+\frac{(x_i+\xi_i)(x_k+\xi_k)}{S^5}\right) \tag{A18}$$

with $\xi_1 = \xi_2 = 0, \xi_3 = \xi$.

The displacement components ω_{kl}^i calculated from (8) are given by:

$$\omega_{11}^1 = \frac{1}{2\pi}\left\{\frac{x_1}{r_4}SA+\frac{x_1^3}{r^6}SB+x_1\xi\left[3(5\alpha-1)\frac{p}{S^5}-15\alpha x_1^2\frac{p}{S^7}\right]+x_1\xi^2\left[-9\alpha\frac{1}{S^5}+15\alpha\frac{x_1^2}{S^7}\right]\right\} \tag{A19}$$

$$\omega_{11}^2 = \frac{1}{2\pi}\left\{\frac{x_2}{r^4}SC+\frac{x_2x_1^3}{r^6}SB+x_2\xi\left[3(3\alpha-1)\frac{p}{S^5}-15\alpha x_1^2\frac{p}{S^7}\right]+x_2\xi^2\left[-3\alpha\frac{1}{S^5}+15\alpha\frac{x_1^2}{S^7}\right]\right\} \tag{A20}$$

$$\omega_{11}^3 = \frac{1}{4\pi}\left\{\frac{D}{r^2}+\frac{x_1^2}{r^4}E+\xi\left[6(1-\alpha)\frac{1}{S^3}+6(3\alpha-1)\frac{p^2}{S^5}+6(\alpha-2)\frac{x_1^2}{S^5}-30\alpha x_1^2\frac{p^2}{S^7}\right]+\xi^2\left[-6\alpha\frac{p}{S^5}+30\alpha x_1^2\frac{p}{S^7}\right]\right\} \tag{A21}$$

$$\omega_{22}^1 = \frac{1}{2\pi}\left\{\frac{x_1}{r^4}SC+\frac{x_1x_2^2}{r^6}SB+x_2\xi\left[3(3\alpha-1)\frac{p}{S^5}-15\alpha x_1^2\frac{p}{S^7}\right]+x_2\xi^2\left[-3\alpha\frac{1}{S^5}+15\alpha\frac{x_1^2}{S^7}\right]\right\} \tag{A22}$$

$$\omega_{22}^2 = \frac{1}{2\pi}\left\{\frac{x_2}{r^4}SA + \frac{x_2^3}{r^6}SB + x_2\xi\left[3(5\alpha-1)\frac{p}{S^5} - 15\alpha x_2^2\frac{p}{S^7}\right] + x_2\xi^2\left[-9\alpha\frac{1}{S^5} + 15\alpha\frac{x_2^2}{S^7}\right]\right\} \quad \text{(A23)}$$

$$\omega_{22}^3 = \frac{1}{4\pi}\left\{\frac{D}{r^2} + \frac{x_2^2}{r^4}E + \xi\left[6(1-\alpha)\frac{1}{S^3} + 6(3\alpha-1)\frac{p^2}{S^5} + 6(\alpha-2)\frac{x_2^2}{S^5} - 30\alpha x_2^2\frac{p^2}{S^7}\right] + \xi^2\left[-6\alpha\frac{p}{S^5} + 30\alpha x_2^2\frac{p}{S^7}\right]\right\} \quad \text{(A24)}$$

$$\omega_{33}^1 = \frac{1}{2\pi}\left\{\frac{x_1}{S^3}F + \frac{x_1\xi}{S^4}G + \frac{x_1\xi^2}{S^5}I\right\} \quad \text{(A25)}$$

$$\omega_{33}^2 = \frac{1}{2\pi}\left\{\frac{x_2}{S^3}F + \frac{x_2\xi}{S^4}G + \frac{x_2\xi^2}{S^5}I\right\} \quad \text{(A26)}$$

$$\omega_{33}^3 = \frac{1}{2\pi}\left\{\frac{1}{S^2}J + \frac{\xi}{S^3}L + \frac{\xi^2}{S^4}M\right\} \quad \text{(A27)}$$

where $A, B, C, D, E, F, G, I, J, L, M$ are polynomials in the variable p/S:

$$A\left(\frac{p}{S}\right) = (\alpha-3+2\beta) + 6(1-\beta)\frac{p}{S} + (5\beta-8\alpha)\frac{p^2}{S^2} + (13\alpha-6-\beta)\frac{p^4}{S^4} + 3(1-2\alpha)\frac{p^5}{S^5} \quad \text{(A28)}$$

$$B\left(\frac{p}{S}\right) = 3(2\beta-\alpha) + 8(\beta-1)\frac{p}{S} + 3(3\alpha-1-2\beta)\frac{p^2}{S^2} + (\beta+8-9\alpha)\frac{p^4}{S^4} + 3(\alpha-1)\frac{p^5}{S^5} \quad \text{(A29)}$$

$$C\left(\frac{p}{S}\right) = (1-\alpha) + 2(1-\beta)\frac{p}{S} + (3\beta-2-4\alpha)\frac{p^2}{S^2} + (11\alpha-4-\beta)\frac{p^4}{S^4} + 3(1-2\alpha)\frac{p^5}{S^5} \quad \text{(A30)}$$

$$D\left(\frac{p}{S}\right) = 2(1-\beta) + 2(3\alpha-5+2\beta)\frac{p}{S} + 2(-9\alpha+7-\beta)\frac{p^3}{S^3} + 6(2\alpha-1)\frac{p^5}{S^5} \quad \text{(A31)}$$

$$E\left(\frac{p}{S}\right) = 4(\beta-1) + 6(2-\alpha-\beta)\frac{p}{S} + 2(6\alpha-7+\beta)\frac{p^3}{S^3} + 6(1-\alpha)\frac{p^5}{S^5} \quad \text{(A32)}$$

$$F\left(\frac{p}{S}\right) = (1-\alpha) - 3\alpha\frac{p^2}{S^2} \quad \text{(A33)}$$

$$G\left(\frac{p}{S}\right) = 3(\alpha+1)\frac{p}{S} - 15\alpha\frac{p^3}{S^3} \quad \text{(A34)}$$

$$I\left(\frac{p}{S}\right) = -3\alpha + 15\alpha\frac{p^2}{S^2} \quad \text{(A35)}$$

$$J\left(\frac{p}{S}\right) = (\alpha-1)\frac{p}{S} - 3\alpha\frac{p^2}{S^2} \quad \text{(A36)}$$

$$L\left(\frac{p}{S}\right) = (1-\alpha) + 3(4\alpha-1)\frac{p^2}{S^2} \quad \text{(A37)}$$

$$M\left(\frac{p}{S}\right) = -9\alpha\frac{p}{S} + 15\alpha\frac{p^3}{S^3}. \quad \text{(A38)}$$

Appendix B

We call $\tilde{\alpha}$, $\tilde{\alpha}_1$ and $\tilde{\beta}$ respectively the coefficients α, α_1 and β in which the substitution $\mu \to \tilde{\mu}(s)$ has been performed. It is noteworthy that the complex variable s in the expression for $\tilde{w}^i_{kk}$ and $\tilde{\omega}^i_{kk}$ appears only in the coefficients $\tilde{\alpha}$, $\tilde{\alpha}_1$ and $\tilde{\beta}$, so that the only Laplace inversions which are needed are:

$$a = L^{-1}\left[\tilde{m}(s)\tilde{g}(s)\tilde{\alpha}(s)\right] \tag{B1}$$

$$a_1 = L^{-1}\left[\tilde{m}(s)\tilde{g}(s)\tilde{\alpha}_1(s)\right] \tag{B2}$$

$$b = L^{-1}\left[\tilde{m}(s)\tilde{g}(s)\tilde{\beta}(s)\right] \tag{B3}$$

$$g_1 = L^{-1}\left[\tilde{m}(s)\tilde{g}(s)\right]. \tag{B4}$$

The quantities $\bar{w}^i_{kk}$ and $\bar{\omega}^i_{kk}$ in the time domain are then:

$$\bar{w}^i_{kk} = a_1 P^i_{kk} + a Q^i_{kk} \tag{B5}$$

$$\bar{\omega}^1_{11} = \frac{1}{2\pi}\left\{\frac{x_1}{r^4} S\ \mathscr{A} + \frac{x_1^3}{r^6} S\ \mathscr{B} + x_1\xi\left[3(5a-g_1)\frac{p}{S^5} - 15ax_1^2\frac{p}{S^7}\right] + x_1\xi^2\left[-9a\frac{1}{S^5} + 15a\frac{x_1^2}{S^7}\right]\right\} \tag{B6}$$

$$\bar{\omega}^2_{11} = \frac{1}{2\pi}\left\{\frac{x_2}{r^4} S\ \mathscr{C} + \frac{x_2 x_1^3}{r^6} S\ \mathscr{B} + x_2\xi\left[3(3a-g_1)\frac{p}{S^5} - 15ax_1^2\frac{p}{S^7}\right] + x_2\xi^2\left[-3a\frac{5}{S^5} + 15a\frac{x_1^2}{S^7}\right]\right\} \tag{B7}$$

$$\bar{\omega}^3_{11} = \frac{1}{4\pi}\left\{\frac{\mathscr{D}}{r^2} + \frac{x_1^2}{r^4}\mathscr{E} + \xi\left[6(g_1-a)\frac{1}{S^3} + 6(3a-g_1)\frac{p^2}{S^5} + 6(a-2g_1)\frac{x_1^2}{S^5} - 30ax_1^2\frac{p^2}{S^7}\right] + \xi^2\left[-6a\frac{p}{S^5} + 30ax_1^2\frac{p}{S^7}\right]\right\} \tag{B8}$$

$$\bar{\omega}^1_{22} = \frac{1}{2\pi}\left\{\frac{x_1}{r^4} S\ \mathscr{C} + \frac{x_1 x_2^2}{r^6} S\ \mathscr{B} + x_2\xi\left[3(3a-g_1)\frac{p}{S^5} - 15ax_1^2\frac{p}{S^7}\right] + x_2\xi^2\left[-3a\frac{1}{S^5} + 15a\frac{x_1^2}{S^7}\right]\right\} \tag{B9}$$

$$\bar{\omega}^2_{22} = \frac{1}{2\pi}\left\{\frac{x_2}{r^4} S\ \mathscr{A} + \frac{x_2^3}{r^6} S\ \mathscr{B} + x_2\xi\left[3(5a-g_1)\frac{p^2}{S^5} - 15ax_2^2\frac{p}{S^7}\right] + x_2\xi^2\left[-9a\frac{1}{S^5} + 15a\frac{x_2^2}{S^7}\right]\right\} \tag{B10}$$

$$\bar{\omega}^3_{22} = \frac{1}{4\pi}\left\{\frac{\mathscr{D}}{r^2} + \frac{x_2^2}{r^4}\mathscr{E} + \xi\left[6(g_1-a)\frac{1}{S^3} + 6(3a-g_1)\frac{p^2}{S^5} + 6(g_1-a)\frac{x_2^2}{S^5} - 30ax_2^2\frac{p^2}{S^7}\right] + \xi^2\left[-6a\frac{p}{S^5} + 30ax_2^2\frac{p}{S^7}\right]\right\} \tag{B11}$$

$$\bar{\omega}^1_{33} = \frac{1}{2\pi}\left\{\frac{x_1}{S^3}\ \mathscr{F} + \frac{x_1\xi}{S^4}\ \mathscr{G} + \frac{x_1\xi^2}{S^5}\ \mathscr{I}\right\} \tag{B12}$$

$$\bar{\omega}^2_{33} = \frac{1}{2\pi}\left\{\frac{x_2}{S^3}\ \mathscr{F} + \frac{x_2\xi}{S^4}\ \mathscr{G} + \frac{x_2\xi^2}{S^5}\ \mathscr{I}\right\} \tag{B13}$$

$$\bar{\omega}^3_{33} = \frac{1}{2\pi}\left\{\frac{1}{S^2}\ \mathscr{I} + \frac{\xi}{S^3}\ \mathscr{L} + \frac{\xi^2}{S^4}\mathscr{M}\right\} \tag{B14}$$

Table B1. Coefficients for the relevant Laplace inversions for the centre of dilation model (see equations (B13), (B16), (B17).

$L^{-1}[\tilde{m}(s)\tilde{g}(s)\tilde{\alpha}(s)]$	$L^{-1}[\tilde{m}(s)\tilde{g}(s)\tilde{\alpha}_1(s)]$	$L^{-1}[\tilde{m}(s)\tilde{g}(s)\tilde{\beta}(s)]$	$L^{-1}[\tilde{m}(s)\tilde{g}(s)]$
$m = 2; \quad n = 1$	$m = 2; \quad n = 1$	$m = 2; \quad n = 1$	$m = 1; \quad n = 0$
$d_1 = -\dfrac{3K(\mu_1+\mu_2)+4\mu_1\mu_2}{(3K+4\mu_1)\eta}$	$d_1 = \dfrac{3K(\mu_1+\mu_2)+4\mu_1\mu_2}{(3K+4\mu_1)\eta}$	$d_1 = -\dfrac{3K(\mu_1+\mu_2)+\mu_1\mu_2}{(3K+\mu_1)}$	$d_1 = 0$
$d_2 = 0$	$d_2 = 0$	$d_2 = 0$	$h_0 = m_0$
$c_1 = -\dfrac{3K(\mu_1+\mu_2)+\mu_1\mu_2}{(3K+\mu_1)\eta}$	$c_1 = -\dfrac{\mu_2}{\eta}$	$c_1 = -\dfrac{3K(\mu_1+\mu_2)+4\mu_1\mu_2}{(3K+4\mu_1)\eta}$	
$h_0 = \dfrac{3K+\mu_1}{3K+4\mu_1} m_0$	$h_0 = \dfrac{3\mu_1}{3K+4\mu_1} m_0$	$h_0 = \dfrac{3K+4\mu_1}{3K+\mu_1} m_0$	

Table B2. Coefficients for the relevant Laplace inversions for the centre of pressure model with SLS rheology (see equations (B14), (B16), (B17)).

$L^{-1}[\tilde{m}(s)\tilde{g}(s)\tilde{\alpha}(s)]$	$L^{-1}[\tilde{m}(s)\tilde{g}(s)\tilde{\alpha}_1(s)]$	$L^{-1}[\tilde{m}(s)\tilde{g}(s)\tilde{\beta}(s)]$	$L^{-1}[\tilde{m}(s)\tilde{g}(s)]$
$m = 3; \quad n = 2$	$m = 1; \quad n = 0$	$m = 3; \quad n = 2$	$m = 2; \quad n = 1$
$d_1 = -\dfrac{\mu_2}{\eta}$	$d_1 = 0$	$d_1 = -\dfrac{\mu_2}{\eta}$	$d_1 = -\dfrac{\mu_2}{\eta}$
$d_2 = 0$	$h_0 = \dfrac{[3K(\mu_1+\mu_2)+4\mu_1\mu_2](\mu_1+\mu_2)}{3\mu_1\mu_2^2} m_p$	$d_2 = 0$	$d_2 = 0$
$d_3 = -\dfrac{3K(\mu_1+\mu_2)+4\mu_1\mu_2}{(3K+4\mu_1)\eta}$	$r = 2; \quad l = 1$	$d_3 = -\dfrac{3K(\mu_1+\mu_2)+\mu_1\mu_2}{(3K+\mu_1)\eta}$	$d_3 = -\dfrac{\mu_1+\mu_2}{\eta}$
$c_1 = -\dfrac{3K(\mu_1+\mu_2)+\mu_1\mu_2}{(3K+\mu_1)\eta}$	$f = -\dfrac{\mu_2}{\eta}$	$c_1 = -\dfrac{3K(\mu_1+\mu_2)+4\mu_1\mu_2}{(3K+4\mu_1)\eta}$	$h_0 = m_p$
$c_2 = -\dfrac{\mu_1+\mu_2}{\eta}$	$e_1 = \dfrac{[3K(\mu_1+\mu_2)^2+3K\mu_2^2+8\mu_1\mu_2^2]\mu_2}{[3K(\mu_1+2\mu_2)+4\mu_1\mu_2]\mu_1\eta}$	$c_2 = -\dfrac{\mu_1+\mu_2}{\eta}$	
$h_0 = \dfrac{3K+\mu_1}{3K+4\mu_1} m_p$	$h_1 = -\dfrac{6K\mu_2+3K\mu_1+4\mu_1\mu_2}{3\mu_2^2} m_p$	$h_0 = \dfrac{3K+4\mu_1}{3K+\mu_1} m_p$	
$h_1 = 0$		$h_1 = 0$	

Table B3. Coefficients for the relevant Laplace inversions for the centre of pressure model with Maxwell solid rheology (see (B1)–(B4), (B16), (B17)).

$L^{-1}[\tilde{m}(s)\tilde{g}(s)\tilde{\alpha}(s)]$	$L^{-1}[\tilde{m}(s)\tilde{g}(s)\tilde{\alpha}_1(s)]$	$L^{-1}[\tilde{m}(s)\tilde{g}(s)\tilde{\beta}(s)]$	$L^{-1}[\tilde{m}(s)\tilde{g}(s)]$
$h_1 = \dfrac{4\mu_1^2}{(3K+4\mu_1)K} m_p$	$h_1 = 0$	$h_1 = -\dfrac{3\mu_1^2}{(3K+\mu_1)K} m_p$	$h_1 = 0$
$h_2 = \dfrac{K-\mu_1}{K} m_p$	$h_2 = \dfrac{3K+4\mu_1}{3\mu_1} m_p$	$h_2 = \dfrac{K+\mu_1}{K} m_p$	$h_2 = m_p$
$h_3 = \dfrac{\mu_1}{\eta} m_p$	$h_3 = \dfrac{6K+4\mu_1}{3\eta} m_p$	$h_3 = \dfrac{\mu_1}{\eta} m_p$	$h_3 = \dfrac{\mu_1}{\eta} m_p$
$h_4 = 0$	$h_4 = \dfrac{K\mu_1}{\eta^2} m_p$	$h_4 = 0$	$h_4 = 0$
$m = 1; \quad n = 0$		$m = 1; \quad n = 0$	
$d_1 = -\dfrac{3K\mu_1}{(3K+4\mu_1)\eta}$		$d_1 = -\dfrac{3K\mu_1}{(3K+\mu_1)\eta}$	

where, if X is a generical polynomial given in Appendix A, we have used italics to denote

$$\mathscr{X}(t) = L^{-1}[\tilde{X}(s)]. \tag{B15}$$

For a centre of dilation the expressions to be inverted in (B1), (B2), (B3) and (B4) can be written as a function $h(s)$:

$$\tilde{h}(s) = \frac{\tilde{p}(s)}{\tilde{q}(s)} + \frac{\tilde{p}_1(s)}{(s-f)^n} = h_0 \frac{(s-c_1)(s-c_2)\ldots(s-c_m)}{(s-d_1)(s-d_2)\ldots(s-d_m)} + h_1 \frac{(s-e_1)(s-e_2)\ldots(s-e_l)}{(s-f)^n} \tag{B16}$$

with $n < m$, $l < n$ and $d_1 \neq d_2 \neq \ldots = d_m$. Their Laplace inverse are given by:

$$h(t) = \sum_{j=1}^{m} \frac{p(d_j)}{q'(d_j)} \cdot \exp(d_j t) + h_1 \exp(ft) \sum_{j=1}^{n} \frac{p_1^{(n-j)}(e_j)\, t^{j-1}}{(n-j)!\,(l-1)!} \tag{B17}$$

where q' is the first derivative and $p_1^{(n-j)}$ is the $(n-j)$-th derivative with respect to s. The coefficients are given in Table 1 for the relevant Laplace inversions.

For a centre of pressure, the expressions to be inverted in (B1), (B2), (B3) and (B4) can be written, as in (B16), as a polynomial $p(s)$ of degree n divided by a polynomial $q(s)$ of degree $m > n$. For a SLS rheology the roots $d_1, d_2, \ldots d_m$ of $q(s)$ are different so that the Laplace inverse can be written as in (B17) (m, n, c_i, d_i are given in Table B2). However, for a Maxwell solid rheology, $q(s)$ has multiple zeros and the quantity to be inverted can be written as:

$$\begin{aligned}\tilde{h}(s) &= \frac{\tilde{p}(s)}{\tilde{q}(s)} + h_2 \frac{1}{s} + h_3 \frac{1}{s^2} + h_4 \frac{1}{s^3} \\ &= h_1 \frac{(s-c_1)(s-c_2)\ldots(s-c_n)}{(s-d_1)(s-d_2)\ldots(s-d_m)} + h_2 \cdot \frac{1}{s_2} + h_3 \cdot \frac{1}{s^3} \quad \frac{1}{s^2} + h_3 \frac{1}{s^3} + h_4 \frac{1}{s^3}\end{aligned} \tag{B18}$$

with $n < m$ and $d_1 \neq d_2 \neq \ldots d_m$. The Laplace inverse of (B18) is then written as:

$$h(t) = \sum_{j=1}^{m} h_1 \frac{p(d_j)}{q'(d_j)} \exp(d_j t) + h_2 H(t) + h_3 t + h_4 \frac{t^2}{2}. \tag{B19}$$

The coefficients c_i, d_i, h_i, m and n are given in Table B3.